Journal of Nonlinear Optical Physics & Materials
Vol. 16, No. 4 (2007) 401–426

World Scientific
www.worldscientific.com

OBSERVATION OF ONE- AND TWO-DIMENSIONAL DISCRETE SURFACE SPATIAL SOLITONS

S. SUNTSOV, K. G. MAKRIS, G. A. SIVILOGLOU, R. IWANOW*,
R. SCHIEK†, D. N. CHRISTODOULIDES and G. I. STEGEMAN

College of Optics and Photonics/CREOL,
4000 Central Florida Blvd, University of Central Florida,
Orlando, Fl, 32816, USA
george@creol.ucf.edu

R. MORANDOTTI

Institut National de la Recherché Scientifique,
Université du Québec, Varennes, Québec, Canada J3X 1S2

H. YANG and G. SALAMO

Physics Department of Physics,
University of Arkansas, Fayetteville, Ark, 72701, USA

M. VOLATIER, V. AIMEZ, and R. ARÈS

Centre de Recherche en Nanofabrication et en Nanocaractérisation,
CRN², Université de Sherbrooke, Sherbrooke,
Québec, Canada J1K2R1

M. SOREL

Department of Electrical and Electronic Engineering,
University of Glasgow, Glasgow, Scotland, G12 8QQ

Y. MIN and W. SOHLER

University of Paderborn, 33095 Paderborn, Germany

XIAOSHENG WANG‡, ANNA BEZRYADINA‡
and ZHIGANG CHEN‡,§

‡*Department of Physics and Astronomy,*
San Francisco State University, CA 94132

§*TEDA Applied Physics School,*
Nankai University, Tianjin 300457 China

Received 26 November 2007

*Intel Corporation, 2200 Mission College Blvd., Santa Clara CA 95052-8119.
†University of Applied Sciences Regensburg, Prüfeninger Str. 58, 93049 Regensburg, Germany.

The recent theoretical predictions and experimental observations of discrete surface solitons propagating along the interface between a one- or two-dimensional continuous medium and a one- or two-dimensional waveguide array are reviewed. These discrete solitons were found in second order (periodically poled lithium niobate) and third order nonlinear media, including AlGaAs, photorefractive media and glass, respectively.

Keywords: Solitons; surface waves; nonlinear optics.

1. Introduction

The optics of light propagation in an array of parallel, identical, weakly coupled waveguides in one- or two-dimensions exhibits many features different from light propagation in a continuous medium.[1] The channels are coupled to each other due to the weak spatial overlap of their fields. In particular, the dispersion relations of the resulting Floquet-Bloch modes yield multiple bands associated with the Brillouin zone of the periodic structure. The first order band (largest allowed propagation wavevector) is separated from the second order band by a forbidden band gap. When a narrow beam is launched into a single channel, modes of the first band are excited and light spreads via "discrete diffraction" throughout the array by tunneling between adjacent waveguides, as shown in Fig. 1(a). For wider beam excitation, the relative phase difference θ between the fields in adjacent channels determines the beam's transverse motion (across the array). More specifically, fields

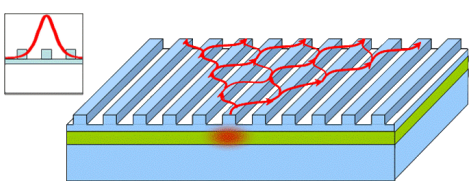

(a)

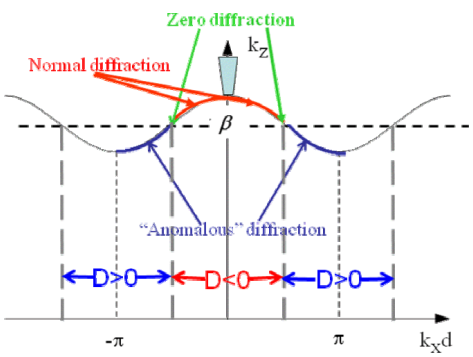

(b)

Fig. 1. (a) The evolution of discrete diffraction throughout an array when a single channel is excited. Inset: Field overlap with adjacent channels. (b) The dispersion relation k_z^{dis} versus $k_x d$ was obtained from coupled mode theory where "d" is the lattice periodicity.

in phase ($\theta = 0,\ \pm 2\pi, \ldots$) or π out-of-phase ($\theta = \pm\pi,\ \pm 3\pi..$) remain centered on the excitation channels, while for intermediate values of θ, the beam's center travels along the array with a transverse Bloch wavevector $k_x = \theta/d$, where d is the periodicity of the array. For the first order band, the propagation wavevector k_z^{dis} varies with θ approximately as $k_z^{dis} = \beta + 2\mathrm{C}\cos(\theta)$, where β is the single, isolated channel propagation wavevector and C is the coupling constant between adjacent channels, see Fig. 1b. Note that diffraction defined as $D = d^2 k_z^{dis}/dk_x^2$ exhibits both normal ($D < 0$) and anomalous ($D > 0$) diffraction for $\pi/2 > |\theta|$ and $\pi > |\theta| > \pi/2$ respectively, Fig. 1(b).

Discrete spatial solitons are electromagnetic wave packets which propagate in a localized manner to a few channels of an array.[1–4] Solitons exist when "discrete diffraction" is arrested by either positive or negative nonlinear phase shifts, which decouple adjacent channels to produce no net power transfer between them. Although the fields in the channels of the array oscillate from maxima to deep minima or zero (due to weak coupling), the envelope of these peaks takes on a solitonic shape, which remains invariant or periodic (breathers) upon propagation. In Kerr media, for "bright" solitons, the product of $\Delta n(I) \times D$ must be negative where $\Delta n(I)$ is an intensity induced change in the refractive index for an intensity I, usually written for the Kerr case as $\Delta n(I) = n_2 I$ (n_2 is the nonlinear Kerr coefficient). Due to the diversity in the sign of the diffraction available in arrays, solitons with no analogue in continuous systems occur. In-phase solitons (fields in phase in adjacent channels) exist for $D < 0$ and $\Delta n > 0$ (self-focusing nonlinearity,[1,4]) at the center ($k_x d = 0$) of the first Brillouin zone. Out-of-phase solitons (fields with a π phase difference between adjacent channels) for $D > 0$ and $\Delta n < 0$ (self-defocusing nonlinearity) occur at the edges ($k_x d = \pm\pi$) of the first Brillouin zone. In fact, such solitons have been observed experimentally inside discrete arrays made of Kerr, photorefractive, quadratic and liquid crystal media for the first time in Refs. 1, 5–10.

Based on theoretical analyses in the 1980's and 1990's of electromagnetic wave propagation along the boundaries between two continuous dielectric media (at least one of which is nonlinear), solitons can be guided by interfaces when the nonlinear index change is of appropriate sign and sufficient magnitude to reverse the initial index difference between the dielectrics.[11–13] For large distances from the interface, the fields decay exponentially into both media. It was predicted then that such self-trapped states would have a power threshold proportional to the initial index difference between the two media, and inversely proportional to the size of the nonlinearity required to cancel this difference. However, to the present date, no experiments have been reported because of the difficulties in finding materials with large enough optically induced index changes to compensate for index differences between available materials. Recently, these concepts were extended to the interface between continuous and periodic media, and surface solitons were predicted with a similar dependence of the power threshold on the index difference between the continuous dielectric medium and that of the periodic array.[14,15]

The special properties of waveguide arrays have now made possible the observation of discrete surface solitons propagating along the boundary between one-dimensional (1D) continuous media (slab waveguides) or two-dimensional (2D) continuous media on the one side and a 1D[16–23] or 2D[24,25] periodic array on the other side. Both the continuous and periodic array regions can be characterized by an effective index $n_{eff,c}$ and $n_{eff,a}$, respectively. Note that because of the higher refractive index in the channel regions, $n_{eff,a} > n_{eff,c}$, the difference $n_{eff,a}$–$n_{eff,c}$ can be varied from zero at the channel waveguide cut-off, to larger values by adjusting the geometry, composition and new channel fabrication techniques.

In this paper, we review the key experiments on surface discrete solitons, and the theoretical papers that stimulated their observation. First, we will consider the simplest case of surface solitons in 1D Kerr media, the underlying basic theory and then the experimental realization. This will then be extended to the 2D case, focusing on the differences with respect to 1D. Next, discrete surface solitons based on the photorefractive nonlinearity (both 1D and 2D) will be summarized, again focusing on the differences from the Kerr case, which is discussed in detail. Finally, the case of quadratic discrete surface solitons, which involve multiple components at different frequencies, will be discussed.

2. Theory of Discrete Surface Solitons in Kerr Media

2.1. *1D Arrays*

To analyze the generic problem of 1D surface solitons, we consider a semi-infinite array as depicted schematically in Fig. 2.[14] Both $n_2 > 0$ and $n_2 < 0$ nonlinearities are considered, with the first being appropriate for AlGaAs at 1550 nm. Since the induced nonlinear index change results in a nonlinear wavevector shift Δk_z^{NL}, which will push the soliton eigenvalue ($n_2 > 0$) into the "forbidden region" (see Fig. 3), the field will decay exponentially into the continuous medium. For $n_2 < 0$, the soliton will be depressed below the dispersion curve into the first forbidden gap between the first and second bands, and again the fields will decay exponentially into the slab waveguide. Therefore, the coupled mode equations for the normalized field amplitudes a_n are given by the discrete nonlinear Schrödinger equation

$$i\frac{da_0}{dZ} + a_1 + |a_0|^2 a_0 = 0, \tag{1a}$$

for the boundary channel $n = 0$, i.e., there is no coupling into a propagating mode of the slab waveguide. For $n \geq 1$, there is coupling to both neighboring channels, and the field evolution with propagation distance is described by

$$i\frac{da_n}{dZ} + (a_{n+1} + a_{n-1}) + |a_n|^2 a_n = 0. \tag{1b}$$

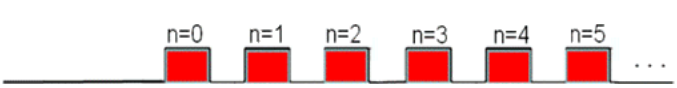

Fig. 2. Schematic representation of the array interface region analysed.

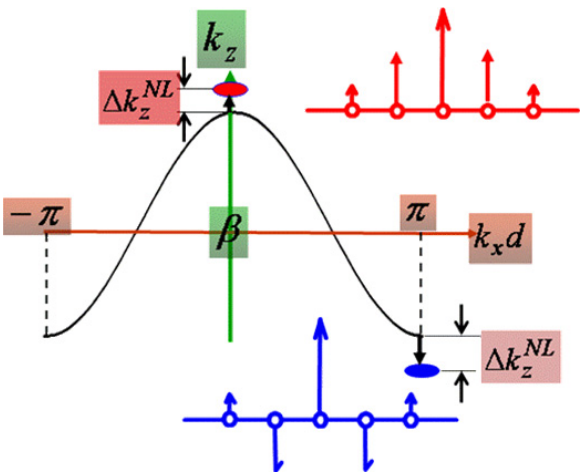

Fig. 3. Eigenvalue location of the corresponding soliton solutions relative to the array's dispersion curve. Red (upper) ellipse is for $n_2 > 0$ and blue (lower) ellipse for $n_2 < 0$. The corresponding Δk_z^{NL} and field distributions are also shown.

The usual propagation co-ordinate z is normalized to the coupling length for discrete diffraction, so that the normalized coordinate Z is given by $Z = Cz$. The dimensionless amplitudes a_n are related to the actual peak electric fields in each channel through the relation $E_n = [(2C\lambda_0\eta_0)/\pi n_2 n_{eff,a}]^{1/2} a_n$, where λ_0 is the free space wavelength and η_0 is the free space impedance.

Understanding the discrete diffraction (linear) behavior of the array is the first step towards solving for the soliton modes. The response to any arbitrary input beam can be determined by the linear superposition of the single channel response functions of the array, weighted by the amplitudes and relative phases imparted by the incident beam. Consider a single waveguide site to be excited at location m from the boundary, that is $a_n(0) = A_0\delta_{nm}$. It has been shown that the field in the nth waveguide of this array at a distance Z from the input is given by[14,16,17,26]:

$$a_n(Z) = A_0[i^{n-m}J_{n-m}(2Z) + i^{n+m}J_{n+m+2}(2Z)]. \tag{2}$$

Figure 4(b) shows the intensity distribution (discrete diffraction) when the first few waveguides ($m = 0$–2) are excited. Clearly, the diffraction patterns in this case differ considerably from those encountered in an infinite array, due to the presence of effective "mirror" sources in the slab waveguide.[26] More specifically, the solution involves an additional term ($J_{n+m+2}(2Z)$) arising essentially from boundary reflections. Finally, sufficiently far from the boundary, i.e., large m, the diffraction behavior approaches that of the infinite array.

Spatial solitons which propagate as a non-diffracting beam along the boundary between a 1D semi-infinite array and a 1D slab waveguide are stationary solutions of Eqs. (1) of the form $a_n = u_n \exp(i[k_z^{dis} + \Delta k_z^{NL}]z)$, where $k_z^{dis} + \Delta k_z^{NL}$ represents the soliton's propagation wavevector, and all the fields u_n are taken to be in-phase (for $n_2 > 0$, $\Delta k_z^{NL} > 0$) and π out-of phase (for $n_2 < 0$, $\Delta k_z^{NL} < 0$)

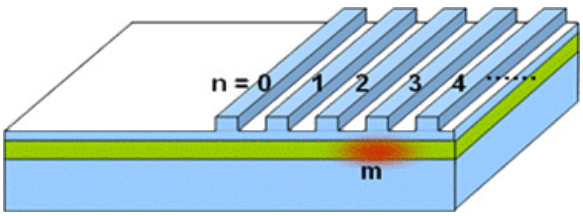

(a)

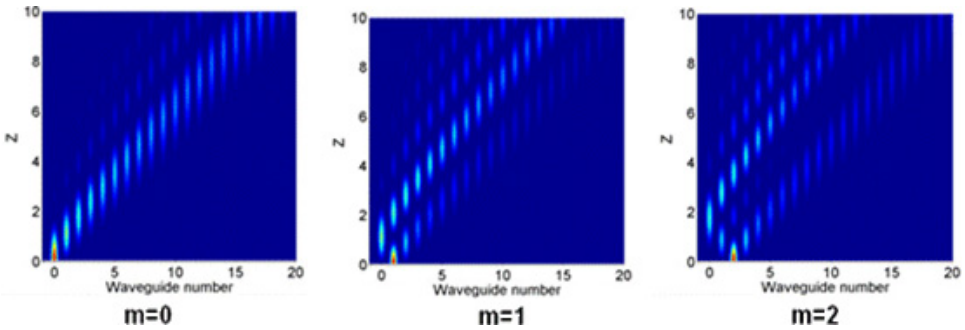

(b)

Fig. 4. (a) Geometry showing the excitation channels defined by m. (b) Discrete diffraction patterns for single channel excitation of $m = 0$, 1 and 2.

with their neighbors a_{n-1} and a_{n+1}. Standard relaxation methods are then used to evaluate the solutions, and the results are plotted in Fig. 5(a) for the total soliton power P versus the nonlinear wavevector increment Δk_z^{NL} associated with these surface solitons for $n_2 > 0$. Note that the results for the two cases, self-focusing and self-defocusing nonlinearity, are essentially mirror images of each other around the axis $\Delta k_z^{NL} = 0$ in Fig. 5(a). Also, there is a power threshold which varies with the channel number n, above which the solitons exist in both cases. The minimum of the existence curves corresponding to the power threshold for solitons peaked in channel n is plotted in Fig. 5(b) as a function of the channel n, i.e., of the distance from the boundary. Linear stability analysis reveals that the negatively sloped $dP/d|\Delta k_z^{NL}| < 0$ part of the $P - |\Delta k_z^{NL}|$ curve, i.e., to the left of the respective minima, are unstable, whereas they are stable to the right where $dP/d|\Delta k_z^{NL}| > 0$ are stable. This behavior indicates that the well-known Vakhitov-Kolokolov criterion valid in the continuum limit for dielectric interfaces is also applicable here.[27–29] Beam propagation techniques were also utilized to verify that the solitons on the $dP/d|\Delta k_z^{NL}| > 0$ branches were indeed stable. This behavior is strongly reminiscent of that obtained previously for nonlinear surface waves at the boundary between two dielectric media, at least one of which is nonlinear.[10–12]

Absolute values for the solution fields at the minimum power threshold are shown Fig. 6(a) for the first few channels from the boundary. Note that the *fields*

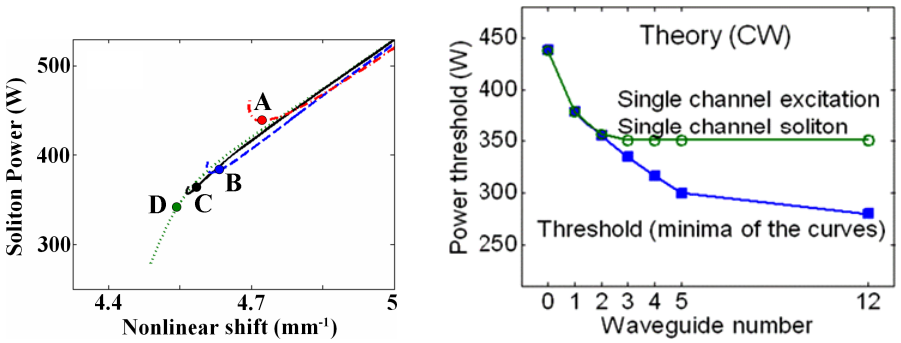

(a) (b)

Fig. 5. (a) The existence curves of power versus normalized nonlinear wavevector for surface solitons in AlGaAs with intensity peaked in the $n = 0, 1, 2$ and 12 channels. The circles labeled A, B, C, and D are the corresponding positions of highly confined surface solitons with approximately the same ratio of the relative intensity of the peak channel to the first neighboring channel. (b) Cw power threshold for soliton formation and the power required to form similar highly confined solitons with single channel excitation.

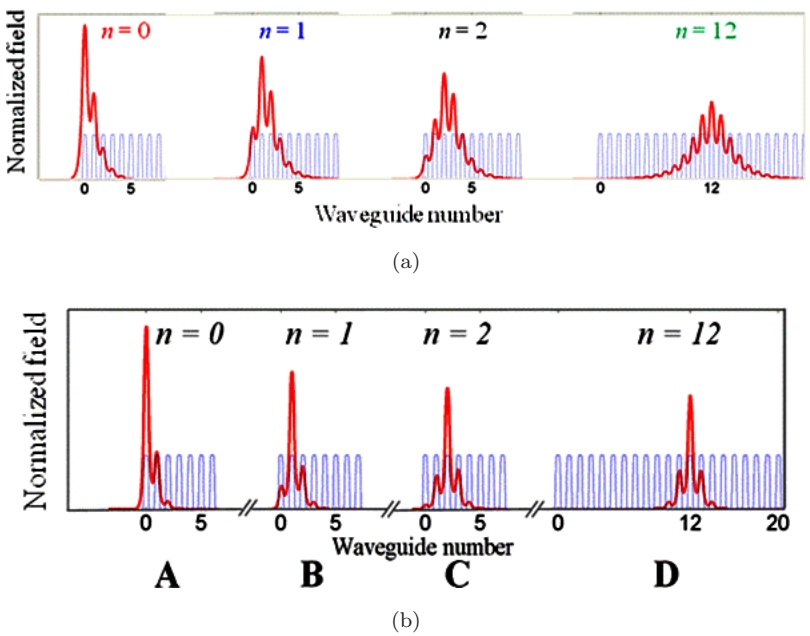

(a)

(b)

Fig. 6. (a) The soliton fields at threshold for various different channels near the boundary at which the soliton is peaked. (b) The strongly confined soliton fields obtained with single channel excitation at a power at which the relative intensity of the first neighbor channel relative to peak intensity channel is approximately the same. The ABCD refer to the points on the dispersion curve shown in Fig. 5(a).

are in-phase or π out-of phase for self-focusing and self-defocusing nonlinearities, respectively. As n, (i.e., the distance from the boundary) increases, the soliton field distributions become less asymmetric, until deep within the array, where they degenerate into the broader solitons of decreasing peak power associated with the solitons that appear in an infinite lattice. However, as the soliton power is increased for a specific n, all solutions that lie on the existence curve become progressively narrower, i.e., more confined around their peak value. In the highly-confined case for the soliton peaked on the boundary channel $n = 0$, the solutions are approximately given by $a_n = A\exp(-np + i[k_z^{dis} + \Delta k_z^{NL}]z)$ where $C(k_z^{dis} + \Delta k_z^{NL}) = A^2 + A^{-2}$ and $p = 2\ln A$.

The solitons deeper into the array become wider, making the diffraction length longer. This makes it more difficult not just to assign a power threshold experimentally, but also to get multiple diffraction length propagation in realistic samples. It proves convenient to define (and measure) the power at which equivalent, strongly confined solitons are reached for each value of n. The variation of the power required with channel number is shown in Fig. 5(b), and the corresponding field distributions in Fig. 6(b). Note, however, that the power thresholds for achieving strongly localized solitons with cw excitation are quite different from the power thresholds associated with the minima in Fig. 5(a) for $n > 3$.

The experiments to be described in the next section were performed with a 1ps pulsed laser in AlGaAs samples with real linear ($\alpha = 0.14$–$0.25\,\mathrm{cm}^{-1}$)[31] and nonlinear (three photon absorption, $\alpha_3 \approx 0.05 \pm 0.02\,\mathrm{cm}^3/GW^2$),[32] Kerr nonlinearity ($n_2 = 1.5 \pm .15 \times 10^{-13}\,\mathrm{cm}^2/W$),[33] and group velocity dispersion ($k" = 1.3 \times 10^{-24}\mathrm{m}^{-1}\mathrm{s}^2$).[31] The sample geometry is shown in Fig 4(a). All of these factors were taken into account to evaluate realistic power thresholds for strongly localized, discrete surface solitons. The results shown in Fig. 7 clearly resemble closely the cw power thresholds corresponding to the minima of the existence curves

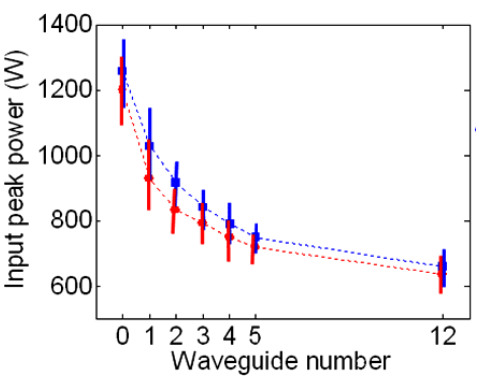

Fig. 7. The threshold power for the strongly localized discrete surface soliton as a function of the channel number, i.e., distance from the surface into the array. Squares (blue) experimental data. Disks (red) simulations based on experimental parameters. The "theoretical" error bars correspond to the uncertainty in the experimentally measured n_2.

shown in Fig. 5(b), except for the elevated peak power values in Fig. 7, due to loss and the pulsed nature of the experiments.

For the 1D case appropriate to gap solutions, Kartashov *et al.* considered in detail the Kerr case for a simple co-sinusoidal refractive index typical of the index modulation found for optically written channels in photorefractive media.[34] Index saturation effects with increasing intensity, also typical of photorefractive nonlinear response, were neglected and surface solitons with fields π out-of-phase in adjacent channels similar to those discussed above were found at the edge of the Brillouin zone. This paper also addressed discrete gap surface solitons associated with higher order bands, and found that their power threshold increased with the band number. Finally, they found twisted gap surface solitons to be unstable.

2.2. *2D Arrays*

In principle, the 2D array case could be analyzed using coupled mode theory in the same way as just discussed for the 1D case. However, the first theoretical paper on 2D discrete solitons utilized the more general Floquet-Bloch analysis.[15] This approach yields the full band structure of the array, and takes into account the exact index structure responsible for waveguiding. A nonlinear Kerr semi-infinite square lattice with a linear refractive index difference between the core and cladding was analysed. The wave propagation in this two-dimensional self-focusing optical lattice is described by the nonlinear Schrödinger equation:

$$i\frac{\partial u(x,y)}{\partial z} + \frac{1}{2k}\left\{\frac{\partial^2 u(x,y)}{\partial x^2} + \frac{\partial^2 u(x,y)}{\partial y^2}\right\} + V(x,y)u(x,y) + \gamma^{(3)}\left|u(x,y)\right|^2 u(x,y) = 0, \tag{3}$$

inside the array ($x \geq 0$) where $V(x,y)$ and $\gamma^{(3)}$ are the normalized semi-infinite index potential and third order nonlinearity respectively.

This analysis leads to the usual discrete solitons belonging to different sites inside the array, and in addition to new soliton solutions at the 90° corners (see Fig. 8(a)), and at each edge between a continuous medium and the 2D array (see Fig. 8(b)). Their properties for the first band are similar to those discussed above for the 1D case. For self-focusing nonlinearities, these solitons lie above (higher values of the propagation wavevector) the first Floquet-Bloch band. The soliton fields travel along the z-axis, and are confined within a few channels along the corner and edge respectively. Again, there are threshold powers for the existence of these solitons, see Fig. 8(c), and the solitons are stable only for positive slopes of the power-nonlinear eigenvector curves. The threshold of the edge surface state is slightly higher than that of the corner soliton, since the latter self-trapped state is confined to fewer sites. Although not discussed in detail in this paper, other surface soliton configurations do exist for different combinations of nonlinearity such as, for example, gap discrete surface solitons etc.[15]

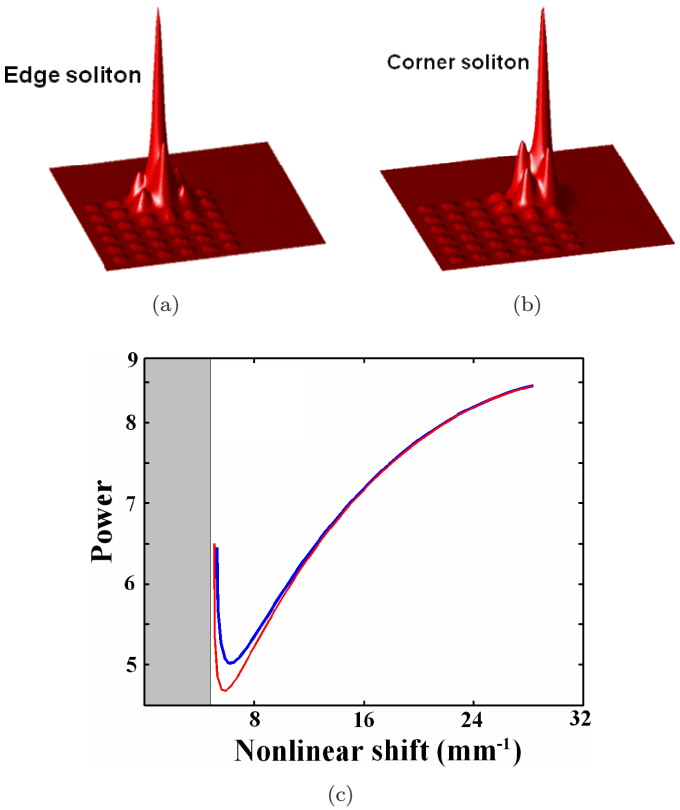

Fig. 8. (a) The field distribution near threshold for an edge discrete spatial soliton for positive Kerr nonlinearity. (b) The field distribution near threshold for a corner discrete spatial soliton for positive Kerr nonlinearity. (c) Normalized power-nonlinear wavevector shift for the edge (red, lower curve) and the corner (blue, upper curve).

3. Experiments on 1D and 2D Kerr Media

3.1. *1D AlGaAs sample*

The sample used for the initial experiments (Fig. 4(a)) had a ridge width $= 4\,\mu$m, periodicity $= 10\,\mu$m, etch depth $= 0.72\,\mu$m, a $1.5\,\mu$m thick core layer of $Al_{0.18}Ga_{0.82}As$ sandwiched between the lower index $Al_{0.24}Ga_{0.76}As$ layers consisting of $0.8\,\mu$m upper cladding and $4\,\mu$m lower cladding layer thicknesses.[16,17,31] The resulting index contrast between the slab waveguide and the array is $\delta \approx 7.5 \times 10^{-4}$.[31] 1ps pulses of wavelength 1550 nm from a 1 KHz OPG/OPA were shaped by circular and cylindrical lenses to match that of the fundamental mode of an isolated waveguide, and then injected into the $n = 0$ channel. The intensity distribution at the output facet of the sample was imaged onto a Roper InGaAs linear array.

The result obtained when the peak power was ramped for small values up to 2 KW is shown in Fig. 9. There are three distinct regions of response. Discrete

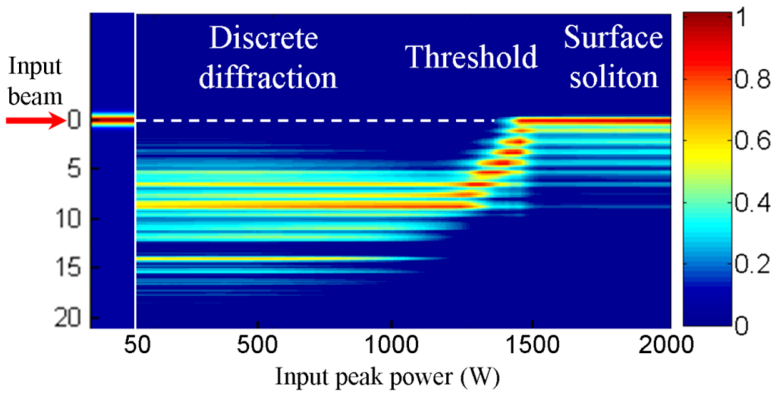

Fig. 9. Intensity distributions recorded at the output facet of the waveguide array sample versus peak power of an input beam injected into the $n = 0$ channel. The output data was sampled for each power by the software, the maximum intensity channel identified, the color of that channel was set to brown (maximum) and the remaining data at that power was renormalized.

diffraction associated with boundary channel excitation persists up to 1 KW power, followed by a rapid collapse of the diffraction pattern into the boundary channel by 1.5 KW and then the strongly localized discrete surface soliton persists up to the highest power levels measured. This rapid collapse is a consequence of the existence of a threshold power for soliton formation, as predicted theoretically. As shown in Fig. 5(a), this threshold corresponds to the minimum in the theoretical existence curve. Finally, as shown in Fig. 10, there is excellent agreement between the measured and theoretically calculated intensity distributions at the output facet.

A new sample was fabricated with the same periodicity (10 μm), variable ridge width (2.4–5.4 μm), etch depth = 1.1 μm (hence index contrast = 2×10^{-3}) and channel length of 1.35 cm. These samples were used to investigate the family of discrete solitons peaked at the $n = 0$, 1, 2, 3, 4, 5 and $n = 12$ channels. The variable ridge width allowed the dependence of the threshold power on the coupling constant to be evaluated. The coupling constants of these samples were measured by analyzing the discrete diffraction patterns deep inside the array, and the results are listed in Table 1. A comparison between experiment and analysis of the structure and modal fields is shown in Fig. 11. Clearly, the agreement is excellent. Note the minimum in coupling length with increasing ridge width. It is a consequence of a trade-off between the stronger confinement that occurs with wider channels, which decreases C, and the overlap of the fields which increases with the width of the channel because of the fixed center-to-center channel separation. The effective nonlinear modal area was calculated from the details of the structure of an isolated channel, and is also listed in Table 1 below.

The threshold power for strongly localized discrete surface solitons was measured for the excitation of the $n = 0$, 1, 2, 3, 4, 5, 12 channels with ridge width = 4.4 μm. In each case, the low power discrete diffraction patterns collapsed into the excitation

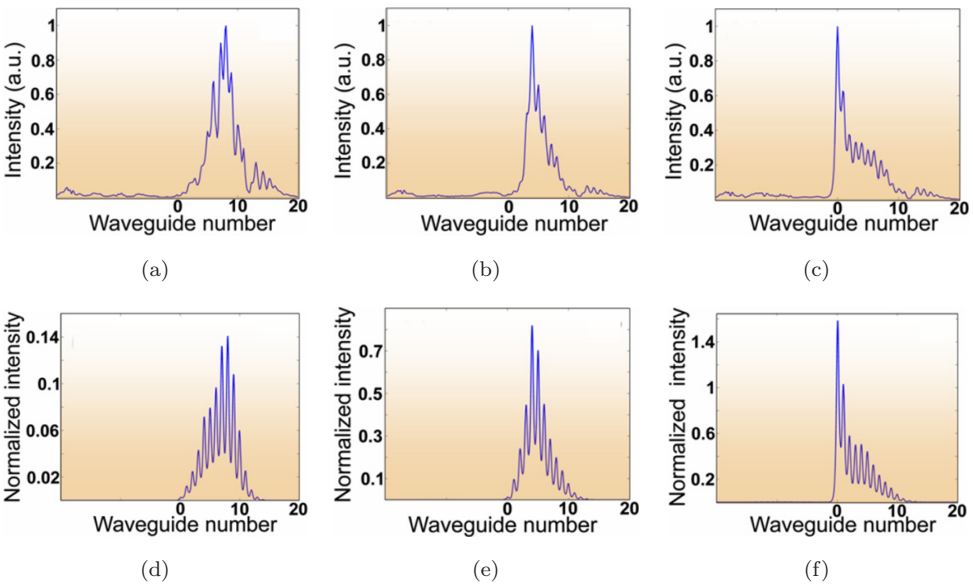

Fig. 10. Measured output intensity when the boundary channel of the waveguide array was excited with a beam of (a) 450 W (low power), (b) 1300 W, and (c) 2100 W peak power. (d), (e) and (f) are the corresponding simulated intensities for 280 W (low power), 1260 W and 2200 W of input power, respectively.

Table 1. Waveguide parameters.

Ridge Width (μm)	Coupling Constant (m^{-1})	Effective Mode Area (μm^2)
2.4	520	17.0
3.4	445	14.8
4.4	420	14.2
5.4	430	14.4

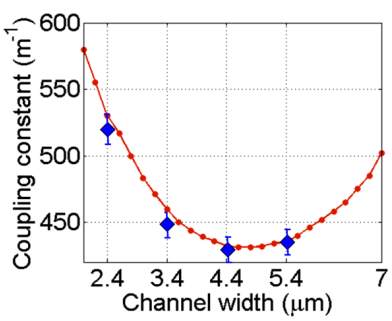

Fig. 11. The dependence of the coupling constant C on the ridge width with fixed center-to-center channel spacing of 10 μm. Data given by diamonds ♦, and calculations by the solid line.

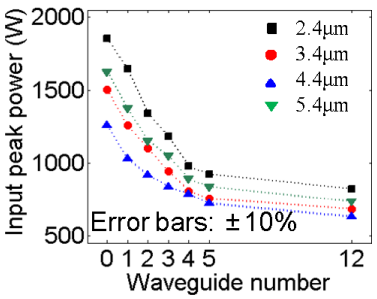

Fig. 12. Input peak power required for a strongly localized soliton formation versus localization site for the samples with $d = 2.4\,\mu$m (squares), $d = 3.4\,\mu$m (circles), $d = 4.4\,\mu$m (triangles), and $d = 5.4\,\mu$m (inverted triangles).

channels as the input power was increased. The variation of the strongly localized discrete soliton's threshold power with n is shown in Fig. 7, along with the results of BPM studies. The agreement is indeed excellent, certainly within the error bars.

The variation in threshold power with increasing n is the same for all the ridge widths studied, i.e., the strongly localized soliton power threshold decreases with n. This is clear from the results shown in Fig. 12. Analogous to a nonlinear two channel coupler, it is expected that the threshold power should vary linearly with C and in fact, the minimum threshold power does coincide with the minimum C.[35] However, the increase in power threshold for the 5.4 μm ridge shown indicates that when the ridge width becomes comparable to the period, other factors also become important.

3.2. *2D Glass sample*

2D arrays were fabricated inside fused silica samples using a novel direct laser writing technique, shown in Fig. 13(a), by researchers at the Fraunhofer Institute in Jena, Germany.[36] A modification of glass and a local increase in the refractive index occurs at the focal point of light from a Ti:sapphire laser focused into the sample. The sample is scanned relative to the laser, and by controlling the pulse energy and the scan rate, the shape and index change could be controlled, producing low-loss waveguides with only a small reduction in the Kerr nonlinearity.[37] Precision arrays consisting of 7×7 channels were fabricated. The ellipticity of the waveguides formed (long axis along the input laser direction, (Fig. 13(b)), was compensated by changing the depth versus lateral spacing of the waveguides, so that the coupling constant C in both the x and y directions is the same. This was checked by measuring the 2D diffraction pattern deep inside the array, and discrete 2D solitons were measured successfully in these samples.[6,38]

Results of experiments on edge and corner discrete surface solitons in these glass waveguide array samples are shown in Fig. 14.[25] The excitation geometry is shown in the upper panel of Fig. 14. The lower panels show the experimental results for the two cases, as well as the theoretical simulations. The low power discrete

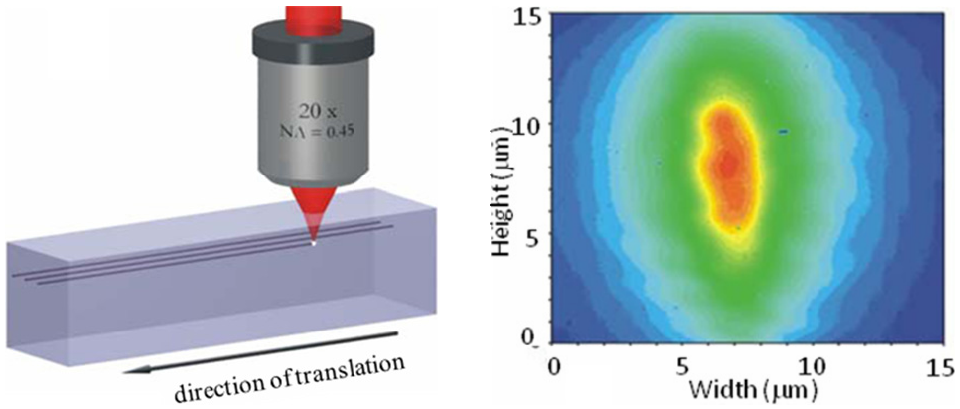

(a) (b)

Fig. 13. (a) Schematic of apparatus used the direct laser writing of arrays of channel waveguides in fused silica (and other materials). (b) Measured mode profile.

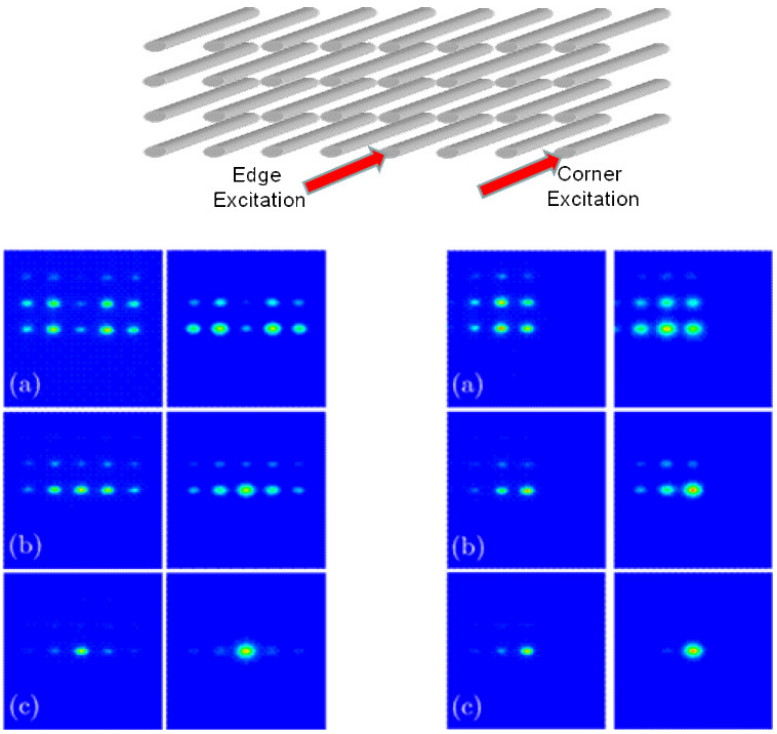

Fig. 14. Upper panel: Single channel excitation geometry for edge (left side) and corner (right side) 2D discrete surface solitons. Lower panel, left side: Left column — experiment, right column — simulation. Excitation of a surface wave along the edge of waveguide array Input peak power is 1.2 MW (a), 1.8 MW (b), and 4.8 MW (c). Lower panel, right side: Left column — experiment, right column — simulation. Excitation of a surface wave along the corner waveguide of the array. Input peak power is 1.2 MW (a), 1.8 MW (b), and 4.8 MW (c).

diffraction patterns for single channel excitation are shown in Fig. 14(a) in the two lower panels for the edge (left side) and corner (right side) respectively. Note the excellent agreement with theory. As the power is increased (b) and (c), localization into the excitation channels increases until in (c), the output intensity distribution of the edge (left lower) and corner (right lower) solitons are obtained.

4. Photorefractive Discrete Surface Solitons: Theory

The photorefractive effect leads to an intensity-dependent refractive index change $\Delta n(I)$ due to a number of physical phenomena.[39] This index change accumulates with absorbed optical flux and saturates at a value determined by the crystal properties and wavelength of illumination. Furthermore, the index change can occur over second or minute, allowing the evolution of a soliton to be monitored as a function of time (i.e., integrated flux).

The screening nonlinearity has been used extensively in demonstrating solitons in discrete media.[1] For an applied electric field along a crystal axis in a noncentrosymmetric crystal, the 1D case yields an intensity-dependent nonlinear index change of the form[39]

$$\Delta n(I) = \frac{\Delta n_0}{1 + (I/I_b)} \tag{4}$$

where I_b is either a dark irradiance proportional to the conductivity of the nonilluminated crystal, or an applied uniform intensity used to increase the conductivity everywhere. Here $\Delta n_0 = \pm 0.5 n_0^3 r_{eff} V/L$. n_0 is the (unperturbed) medium index, r_{eff} is the effective electro-optic tensor component, and V is the voltage applied to the crystal electrodes separated by distance L. Note that the nonlinearity can be either self-focusing or self-defocusing depending on the voltage applied. This expression was also a good approximation for the 2D case used in obtaining a 2D discrete surface soliton.[24]

A second form of photorefractive nonlinearity used in discrete surface soliton experiments is the photovoltaic nonlinearity used in titanium in-diffused $LiNbO_3$ channel waveguides used for 1D discrete arrays. The waveguides are made by in-diffusion of copper or titanium through masks deposited on the surface. The nonlinearity is of the defocusing type, and the saturating index change is given by

$$\Delta n(I) = \Delta n_0 \frac{I/I_b}{1 + (I/I_b)} \tag{5}$$

where $\Delta n_0 = -0.5 n_0^3 r_{eff} \kappa / q \mu \tau_R$. κ is the material's photovoltaic constant, q is the charge on the electron, and τ_{R} is the carrier recombination time. This nonlinearity was used to demonstrate 1D discrete surface gap solitons.[19–21]

The analysis of surface discrete solitons in photorefractive media closely mirrors that of Kerr media, with the Kerr law nonlinearity replaced by an appropriate saturating one, Eq. (4) or (5). For the 2D array case, the pertinent propagation

equation is

$$i\frac{\partial u(x,y)}{\partial z} + \frac{1}{2k}\left\{\frac{\partial^2 u(x,y)}{\partial x^2} + \frac{\partial^2 u(x,y)}{\partial y^2}\right\} + V(x,y)u(x,y) + \Delta n(I)|u(x,y)|^2 u(x,y) = 0. \quad (6)$$

Translating to the 1D case, $u(x,y)$ and $V(x,y)$ are replaced by $u(x)$ and $V(x)$ respectively, and there is no diffraction term along the y-axis. The solutions again exhibit in-phase soliton fields for adjacent channels at the center of the Brillouin zone and π out-of-phase soliton fields between adjacent channels at the edge of the Brillouin zone.

5. Experiments on Discrete Surface Solitons in Photorefractive Media

5.1. *1D Discrete gap solitons*

Two very similar experiments which demonstrate discrete 1D gap surface solitons have been reported based on the photovoltaic effect in $LiNbO_3$ waveguide arrays.[19–21] Both samples used x-cut surfaces with propagation along the y-axis. Titanium in-diffusion through a mask was used to create the weakly coupled, individual, single mode channels. To increase the photorefractive response, either Fe or Cu was also diffused in through the x-cut surface.[19] Light in the blue-green part of the spectrum, polarized along the z-axis (TE-polarized), was injected into single boundary channels, and the intensity distribution at the output facet was measured.

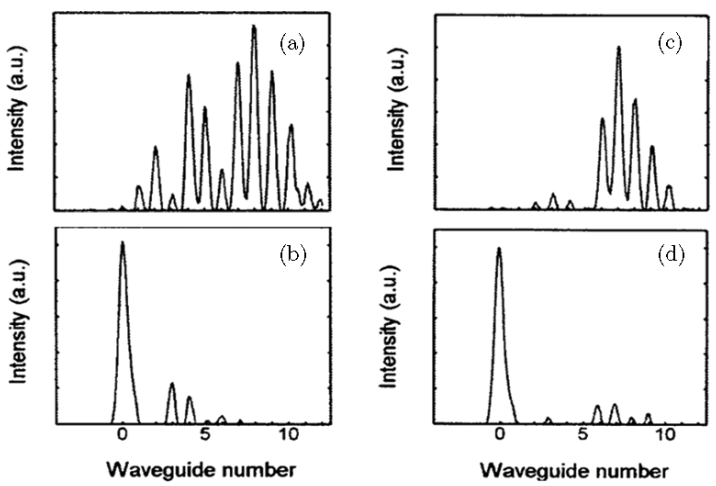

Fig. 15. Intensity distributions observed at the output facet of photovoltaic $LiNbO_3$ sample for single (a) and (b) channel and three (c) and (d) channel excitation (intensity ratios 1.0:0.5:0.1 for $n = 0$, 1 and 2 respectively) at low (a) and (c), and high powers of 0.225 mW (b) and 0.45 mW (d) respectively.[19]

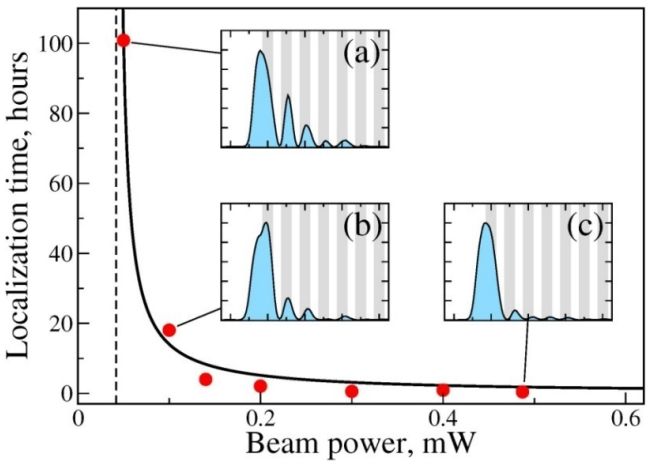

Fig. 16. Measured surface localization time vs probe beam power. Solid curve: $A+B/(P-P_{th})$ fit to experimental data (red dots). Vertical dashed line marks the threshold power ($P_{th} = 0.042$ mW). (a)–(c) Beam intensity profiles of decreasing width corresponding to the indicated points.

Typical results are shown in Figs. 15 and 16. The first shows both the low power diffraction patterns of single channel and three channel excitation at low powers.[18] For the three channel case, the input beam was tilted to produce a π phase difference between adjacent channels. With increasing input power, these patterns both collapsed into a discrete surface soliton peaked on the boundary channel ($n = 0$). Agreement with simulations in both reports was very good.[19–21]

A demonstration of the existence of a threshold power for surface discrete soliton formation is shown in Fig. 16.[20] It relies on the well-known fact that the final steady state change in refractive index decreases with decreasing intensity of illumination. A threshold power corresponds to a threshold change in the refractive index in the boundary channel for soliton formation. It is clear in Fig. 16 that there is a minimum input power required for soliton formation, since the formation time diverges at a power of 0.42 mW.

Very recently, the trapping via a combination of self- and cross-phase modulation was reported at a surface channel of a continuum excited in a photonic crystal fiber with a femtosecond Ti:-sapphire source.[21] The nonlinearity was the photovoltaic effect in a 1D photorefractive titanium in-diffused $LiNbO_3$ array of channel waveguides as described above.

5.2. *2D Discrete surface solitons*

An experiment using the screening nonlinearity in the photorefractive Ce:SBN was published[24] almost simultaneously with the Kerr nonlinearity ($n_2 > 0$) glass experiments discussed in Sec. 3.2. Because the sign of the nonlinearity is easily changed for the screening nonlinearity, surface solitons at both the Brillouin zone center and

edge (gap solitons) were demonstrated. The photorefractive results for the positive nonlinearity using single channel excitation were very similar to those already shown in Fig. 14 for the glass samples.

The waveguides were fabricated using the optical induction technique.[40] Partially incoherent light is transmitted through an amplitude mask onto the crystal entrance facet, resulting in a square lattice pattern with a sharp edge/corner after appropriate imaging. A cross-polarized (to the writing beam) Gaussian beam at 488 nm, shaped to the single channel mode profile, was focused onto the edge or corner channel of interest at normal incidence, and the light intensity pattern at the output facet was recorded.

The experimental results for both signs of the effective nonlinearity are shown in Fig. 17. The lattice structure is shown in Fig. 17(a). The panels (b)–(d) and (e)–(g) are for self-focusing and self-defocusing cases, respectively. Note that the gap soliton is not as strongly localized (e) as the one at the center of the Brillouin zone (b). The key results are shown in Figs. 17(c) and (f), in which the interference patterns between the soliton outputs from the crystal and a plane wave are recorded. For the self-focusing case, the bright spots corresponding to neighboring channels are clearly in-phase with one another. However, the bright spots are out-of-phase for the defocusing case, i.e., every adjacent channel experiences destructive interference, indicating a π phase shift between channels. The last column (d) and (g) shows a comparison of the wavevector spectrum measured via "Brillouin zone spectroscopy" for the self-focusing and self-defocusing cases.[41] Clearly, both varieties of edge discrete surface solitons have been observed.

6. Coupled Mode Theory of Discrete Surface Solitons: Quadratic Media

There are two unique features associated with using quadratic nonlinearities to create spatial solitons. One, the effective nonlinearity can either be of the self-focusing or self-defocusing type.[44] Defining the isolated channel guided wave propagation constants as $\beta(\omega)$ and $\beta(2\omega)$ for the fundamental and harmonic fields respectively for Second Harmonic Generation (SHG), $\Delta\beta = 2\beta(\omega) - \beta(2\omega)$, the wavevector mismatch for second harmonic generation determines the sign of the nonlinearity. Self-focusing occurs for $\Delta\beta > 0$, and self-defocusing for $\Delta\beta < 0$. Thus by tuning $\Delta\beta$, it is possible to study discrete surface solitons at both the center and edge of the first Brillouin zone. Second, the soliton consists of 2–3 different frequency components, all strongly coupled via the second order nonlinearity $\chi^{(2)}_{ijk}(-[\omega_1 \pm \omega_2]; \omega_1, \omega_2)$. All of the frequency components propagate locked together with the same phase and group velocity.

The locking of frequency components which differ by at least a factor of two in frequency seriously impacts the discrete diffraction process, since the coupling constant is a very strong function of frequency. A typical SHG sample exhibits drastically different field confinements for the fundamental and harmonic. This

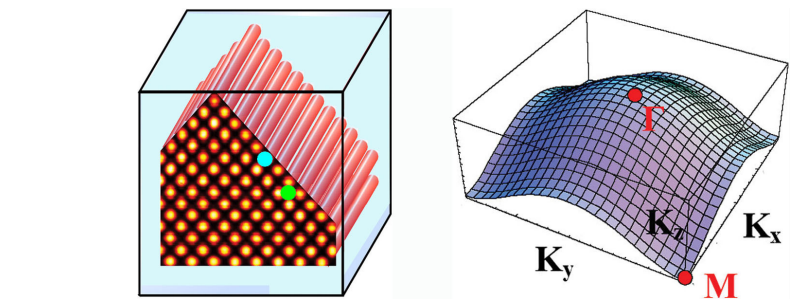

(a)

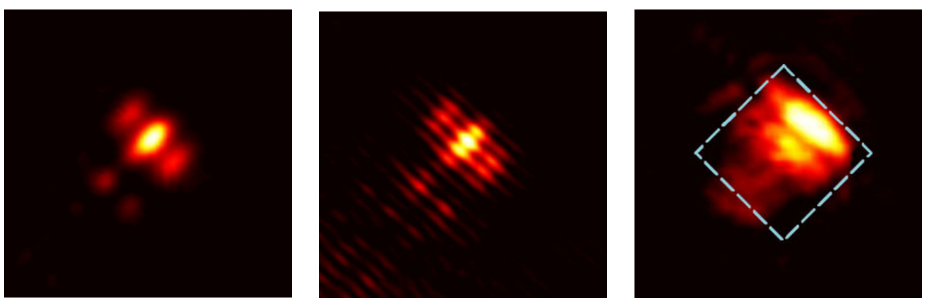

(b) (c) (d)

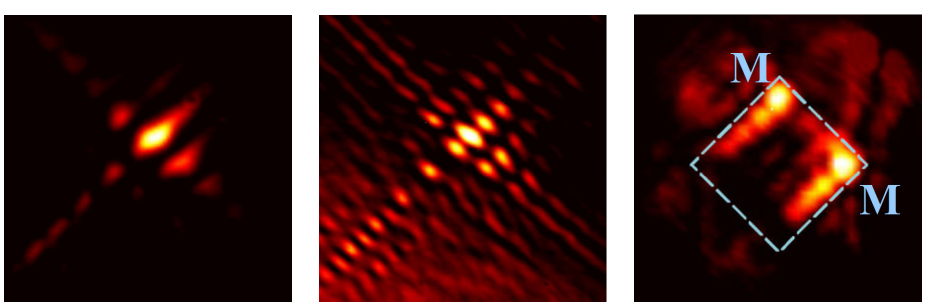

(e) (f) (g)

Fig. 17. Results of the experiments showing the excitation of both Brillouin zone center (in-phase fields in adjacent channels) and edge (π out-of-phase fields in adjacent channels) 2D discrete surface solitons in a photorefractive crystal. (a) Left panel: Illustration of the optically induced lattice surface, where the probe beam location is marked by a blue (green) spot for excitation of in-phase (out-of-phase) surface solitons; Right panel: Dispersion relation for the first Floquet-Bloch band showing the Γ point where in-phase solitons exist and the M point where π out-of-phase solitons occur. (b), (c) and (d) are for in-phase solitons and (e), (f) and (g) for out-of-phase solitons. (b) and (e) show the soliton intensity distributions at the output facet. (c) and (f) show interference patterns between the soliton outputs and a plane wave. (d) and (g) show spatial spectra when the probe beam undergoes nonlinear self-trapping. (The blue squares mark the edge of the first Brillouin Zone).

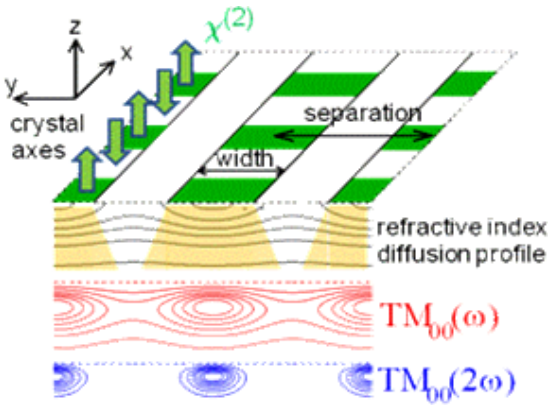

Fig. 18. Cross-section of the periodically poled $LiNbO_3$ sample showing the periodic poling inversion of $\chi^{(2)}_{333}$, the titanium in-diffusion profile and the resulting index profile, the width and separation of the guiding channels, and the fundamental $TM_{00}(\omega)$ and harmonic $TM_{00}(2\omega)$ field distributions.

is shown in Fig. 18 for the periodically poled $LiNbO_3$ samples used. When this process is near phase-match ($\Delta\beta = 0$), there is effectively no discrete diffraction experienced by the harmonic wave due to its strong confinement. As a result, the only source of SH fields in a channel is the generation via the SHG process. The relevant nonlinear equations for the fundamental u_n and harmonic v_n field envelopes are given by[4]:

$$-\Delta k_z^{sol} u_n + C[u_{n+1} + u_{n-1}] + \frac{2}{2\Delta k_z^{sol} + \Delta\beta}|u_n|^2 u_n = 0$$

$$v_n = \frac{2}{2\Delta k_z^{sol} + \Delta\beta} u_n^2 \quad n \geq 1$$

$$-\Delta k_z^{sol} u_0 + C u_1 + \frac{2}{2\Delta k_z^{sol} + \Delta\beta}|u_0|^2 u_0 = 0$$

$$v_0 = \frac{2}{2\Delta k_z^{sol} + \Delta\beta} u_0^2 \quad n = 0.$$

Again, there are minimum threshold powers in the power-eigenvalue existence curves for discrete quadratic surface solitons, as shown in Fig. 19. The above equations suggest the four possibilities shown in Fig. 19. Consider first $2\Delta k_z^{sol} > 0$, and the soliton is located above the fundamental's dispersion curve, the effective nonlinearity is self-focusing for $2\Delta k_z^{sol} + \Delta\beta > 0$, the fundamental and harmonic fields are in phase from channel to channel and with one another, and the fundamental field is larger than the harmonic one (Case A). However, if $\Delta\beta$ is negative with its magnitude smaller than $2\Delta k_z^{sol}$, the effective nonlinearity is still of the self-focusing type, and this soliton is characterized by dominant harmonic fields (Case B). If $2\Delta k_z^{sol} < 0$ and the soliton is located below the fundamental's dispersion curve, the effective nonlinearity is self-defocusing for $2\Delta k_z^{sol} + \Delta\beta < 0$, the

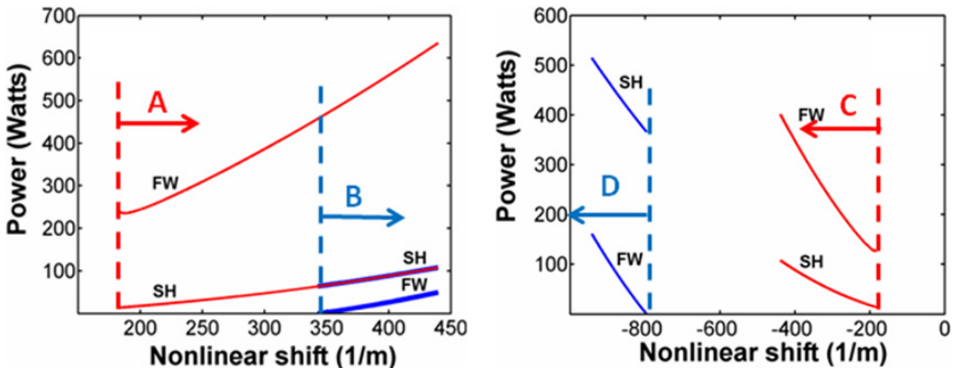

Fig. 19. Existence (power-eigenvalue) curves for the fundamental and harmonic components of the quadratic discrete surface solitons for all four cases A, B (a), C, D (b) described in the text. In (a), the SH for case A is identical with Case B after the threshold for B. $\Delta\beta L = +36\pi$ for A and D, and $\Delta\beta L = -15\pi$ for B and C. The dashed vertical lines are the threshold for the cases indicated. The total soliton power consists of the FW + SH.

fundamental fields are π out-of-phase from channel to channel, the harmonic fields are in-phase from channel to channel and the fundamental field dominates, Case C. When $\Delta\beta > 0$ and smaller in magnitude than $2\Delta k_z^{sol}$, the effective nonlinearity is again self-defocusing, but the harmonic field is now dominant (Case D).

7. Experiments on 1D Quadratic Media (PPLN Samples)

The sample geometry and resulting field distributions were shown in Fig. 18. The regions in which Ti was in-diffused were 7 μm wide, and the center-to-center channel spacing was varied from 14–16 μm for different arrays. The array used for experiments had a channel-to-channel period that was chosen to give a $L_c = 15.74$ mm coupling length. In the current case, the maximum refractive index change due to Ti in-diffusion was $\Delta n < 8 \times 10^{-3}$. Each array consisted of 101 identical guides, and the samples were 5 cm long. The periodic poling period was 16.8 μm, which produced phase match ($\Delta\beta = 0$) at a temperature of 234°C. Raising the temperature decreased $\Delta\beta$, and an oven was used to attain the desired phase-mismatch. The measured loss for the fundamental wave was 0.15 dB/cm and 0.30 dB/cm for the harmonic. A 2-year development program at the University of Paderborn was required to achieve uniform phase-match across the central part of the array. The key was to fabricate arrays with channels for which the second harmonic wavelength peak response in neighboring channels varied only by small wavelength changes, smaller than the SHG bandwidth of individual channels. These arrays were previously used to observe quadratic solitons near the middle of the arrays, and their characterization can be found in Ref. 42.

The apparatus used to excite the arrays was more demanding than that for the AlGaAs samples because of the very narrow SHG bandwidths of the channels, which were measured to fall in the range of 0.25–0.30 nm (corresponding to a bandwidth limited pulse width of 10-8 ps respectively) with a low power, tunable, single frequency 1550 nm diode laser. To achieve the right combination of power and bandwidth, a 5 MHz repetition rate pulsed fiber laser from Pritel was stretched in the chirped fiber grating, amplified in a large core EDFA, and then recompressed with a pair of bulk gratings to 7.7 ps, bandwidth limited (0.22 nm) pulses with maximum peak power of 4 kW. The bulk, high efficiency, grating pulse compressor limited the source tuning range to 1554–1561 nm.

Experiments on discrete surface soliton generation were performed by the excitation of the boundary channel with the fundamental beam. The incident beam was shaped to match as closely as possible to the fundamental mode profile of an isolated channel. This method of excitation favors the excitation of solitons with the fundamental as the dominant frequency, the cases A and C discussed above.

The results for both $\Delta\beta > 0$ and $\Delta\beta < 0$ are shown in Fig. 20. Although the region labeled "bulk" is also periodically poled and could in principle support second harmonic generation, the phase-mismatch is very large, since the experiment was operated near phase-match for the channel waveguides. Hence, there is insufficient SH generated in the "bulk" to support quadratic spatial solitons there. As a result, this case corresponds to surface solitons guided by the interface between a 1D semi-infinite array and a semi-infinite 2D half-space. This is in contrast to the Kerr case previously discussed, for which discrete surface solitons were guided by the interface

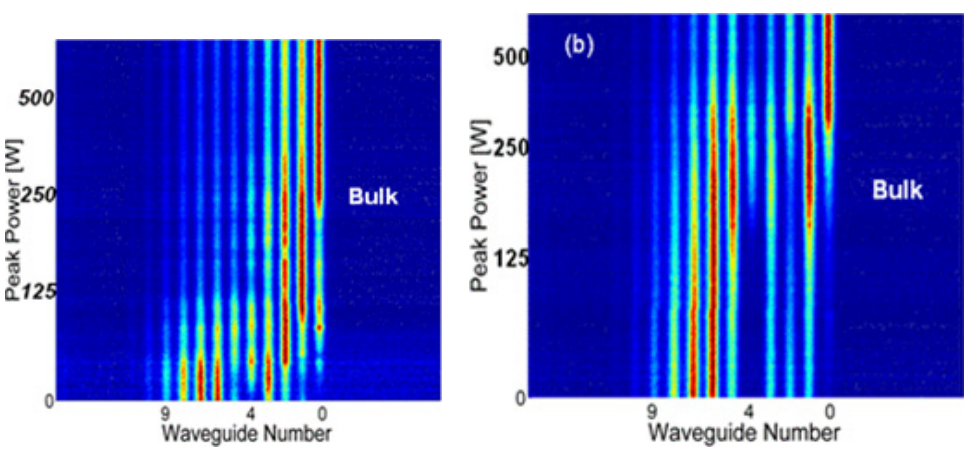

Fig. 20. Intensity distribution measured at the output facet when the boundary channel is excited with increasing fundamental input power. (a) $\Delta\beta L = +36\pi$. (b) $\Delta\beta L = -15.5\pi$. "Bulk" represents a crystal region which is also periodically poled but there is no waveguide confinement.

between a 1D semi-infinite periodic medium and a 1D semi-infinite medium (slab waveguide).

In both cases, the discrete diffraction patterns collapse into discrete surface solitons at around 500 W peak input fundamental power, shown in Fig. 20. Note that because the magnitude of the phase-mismatch is larger for $\Delta\beta > 0$ than for $\Delta\beta < 0$, the magnitude of the effective nonlinearity is larger for the "gap" soliton case. As a result, the confinement to the boundary channel is higher for the gap case. Note that the BPM simulated intensity patterns at the output facet based on the theoretical equations are in good agreement with the experimentally measured ones, as shown in Fig. 21. However, the lack of discrete diffraction for the harmonic and the single boundary channel excitation with only the fundamental, results in large differences in the FW and SH intensity distributions at the output facet. Although there are large "tails" extending up to channel 9 for the fundamental wave, the SH is confined to the first 2–3 channels. This occurs because of a combination of

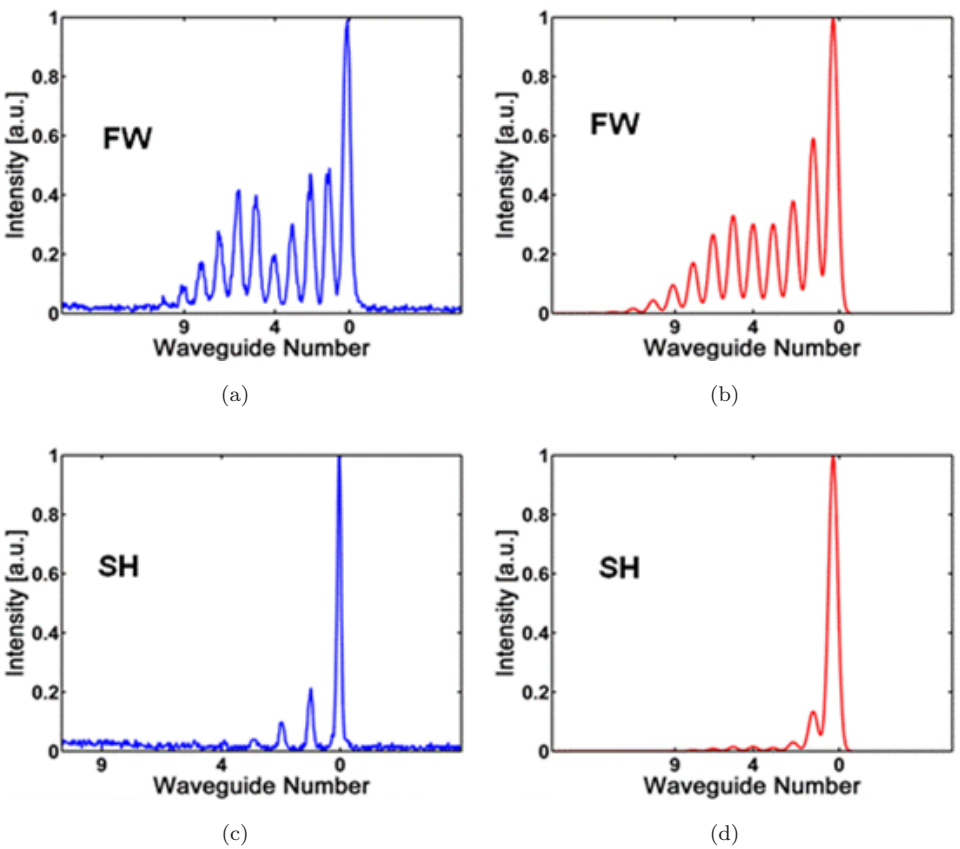

Fig. 21. Measured, (a) and (c), and calculated, (b) and (d), field distributions for the "gap" discrete surface soliton at the sample output facet for the fundamental, (a) and (b), and harmonic, (c) and (d), soliton components.

the fundamental intensity in the channels and the distance over which the SH can grow, i.e., a number of discrete diffraction distances must take place before the SH can grow in the outer channels.

8. Summary

We have described the first successful experiments on the generation of surface solitons travelling along the interface between a periodic medium and a 1D and 2D semi-infinite medium. Discrete surface solitons lying at the center and the edge ("gap" solitons) of the first Brillouin zone have been investigated in Kerr, photorefractive and quadratically nonlinear media. As predicted theoretically, these solitons have power thresholds and in general, the agreement between experiment and theory was excellent.

Finally, we note that the claims made in Ref. 45 that the authors of that article were the first to report the observation of "nonlinear Tamm states", "discrete soliton gap states", and "surface discrete solitons" in general are false.[20] In fact, their work was preceded by Refs. 16–19, with the earliest dating back over one year prior to their work.[16,17]

References

1. D. N. Christodoulides, F. Lederer and Y. Silberberg, Discretizing light behaviour in linear and nonlinear waveguide lattices, *Nature* **424** (2003) 817–823.
2. D. N. Christodoulides and R. I. Joseph, Discrete self-focusing in nonlinear arrays of coupled waveguides, *Opt. Lett.* **13** (1988) 794–796.
3. Y. S. Kivshar, Self-localization in arrays of defocusing waveguides, *Opt. Lett.* **18** (1993) 1147–1149.
4. F. Lederer, S. Darmanyan and A. Kobyakov, Discrete Solitons, in *Spatial Solitons*, eds. S. Trillo and W. Torruellas, Springer Series on Optical Sciences, Vol. 82 (Springer, New York, 2001).
5. H. S. Eisenberg, Y. Silberberg, R. Morandotti, A. R. Boyd and J. S. Aitchison, Discrete spatial optical solitons in waveguide arrays, *Phys. Rev. Lett.* **81** (1998) 3383–3386.
6. A. Szameit, J. Burghoff, T. Pertsch, S. Nolte, A. Tuennermann and F. Lederer, Two-dimensional soliton in cubic fs laser written waveguide arrays in fused silica, *Opt. Expr.* **14** (2006) 6055–6062.
7. J. W. Fleischer, T. Carmon, M. Segev, N. K. Efremidis and D. N. Christodoulides, Observation of discrete solitons in optically induced real time waveguide arrays, *Phys. Rev. Lett.* **90** (2003) 023902.
8. J. W. Fleischer, M. Segev, N. K. Efremidis and D. N. Christodoulides, Observation of two-dimensional discrete solitons in optically induced nonlinear photonic lattices, *Nature* **422** (2003) 147–150.
9. R. Iwanow, R. Schiek, G. I. Stegeman, T. Pertsch, F. Lederer, Y. Min and W. Sohler, Observation of discrete quadratic solitons, *Phys. Rev. Lett.* **93** (2004) 113902.
10. A. Fratalocchi, G. Assanto, K. A. Brzdakiewicz and M. A. Karpierz, Discrete propagation and spatial solitons in nematic liquid crystals, *Opt. Lett.* **29** (2004) 1530–1532.

11. A. Maradudin, Nonlinear surface electromagnetic waves, in *Optical and Acoustic Waves in Solids-Modern Topics* (World Scientific, Singapore, 1983), Chap. 2, pp. 72–142.
12. N. N. Akhmediev, V. I. Korneev and Y. V. Kuz'menko, Excitation of nonlinear surface waves by Gaussian light beams, *Sov. Phys. JETP* **61** (1985) 62–67.
13. A. D. Boardman, P. Egan, F. Lederer, U. Langbein and D. Mihalache, Third-order nonlinear electromagnetic TE and TM guided waves, in *Nonlinear Surface Electromagnetic Phenomena*, eds. H. E. Ponath and G. I. Stegeman (North-Holland, Amsterdam, 1991), pp. 73–287.
14. K. G. Makris, S. Suntsov, D. N. Christodoulides, G. I. Stegeman and A. Hache, Discrete surface solitons, *Opt. Lett.* **30** (2005) 2466–2468.
15. K. Makris, J. Hudock, D. N. Christodoulides, G. I. Stegeman, O. Manela and M. Segev, Surface lattice solitons, *Opt. Lett.* **31** (2006) 2774–2776.
16. S. Suntsov, K. G. Makris, D. N. Christodoulides, G. I. Stegeman, A. Hache, R. Morandotti, H. Yang, G. Salamo and M. Sorel, Nonlinear Tamm states in waveguide lattices, OSA Topical meeting on nonlinear guided wave phenomena (Digest of NLGW 2005, Optical Society of America, Washington, 2005), Dresden Germany, September 2005, paper ThC4.
17. S. Suntsov, K. G. Makris, D. N. Christodoulides, G. I. Stegeman, A. Hache, R. Morandotti, H. Yang, G. Salamo and M. Sorel, Observation of discrete surface solitons, *Phys. Rev. Lett.* **96** (2006) 063901.
18. G. A. Siviloglou, K. G. Makris, R. Iwanow, R. Schiek, D. N. Christodoulides, G. I. Stegeman, Y. Min and W. Sohler, Observation of discrete quadratic surface solitons, *Opt. Expr.* **14** (2006) 5508–5516.
19. E. Smirnov, M. Stepic, C. E. Ruter, D. Kip and V. Shandarov, Observation of staggered surface solitary waves in one-dimensional waveguide arrays, *Opt. Lett.* **31** (2006) 2338–2340.
20. R. Rosberg, D. N. Neshev, W. Krolikowski, A. Mitchell, R. A. Vicencio, M. I. Molina and Yu. S. Kivshar, Observation of surface gap solitons in semi-infinite waveguide arrays, *Phys. Rev. Lett.* **97** (2006) 083901.
21. A. Sukhorukov, D. N. Neshev and Y. S. Kivshar, Shaping and control of polychromatic light in nonlinear photonic lattices, *Opt. Expr.* **15** (2007) 13058–13076.
22. S. Suntsov, K. G. Makris, D. N. Christodoulides, G. I. Stegeman, R. Morandotti, H. Yang, G. Salamo and M. Sorel, Power thresholds of families of discrete surface solitons, *Opt. Lett.* **32** (2007) 3098–3100.
23. G. Stegeman, D. Christodoulides, S. Suntsov, K. Makris, G. Siviloglou, R. Schiek, R. Morendotti, A. Haché, H. Yang, G. Salamo, M. Sorel, Y. Min and W. Sohler, Spatial solitons at the interface between discrete and continuous media, in *Proc. of SPIE 14th International School on Quantum Electronics: Laser Physics and Applications*, eds. Peter A. Atanasov, Tanja N. Dreischuh, Sanka V. Gateva and Lubomir M. Kovachev, Vol. 66041C (SPIE, USA, 2007).
24. X. Wang, A. Bezryadina, Z. Chen, K. G. Makris, D. N. Christodoulides and G. I. Stegeman, Observation of two-dimensional surface solitons, *Phys. Rev. Lett.* **98** (2007) 123903.
25. Szameit, Y. V. Kartashov, F. Dreisow, T. Pertsch, S. Nolte, A. Tünnermann and L. Torner, Observation of two-dimensional surface lattice solitons, *Phys. Rev. Lett.* **98** (2007) 173903.
26. K. G. Makris and D. N. Christodoulides, Method of images in optical discrete systems, *Phys. Rev. E* **73** (2006) 036616.
27. N. G. Vakhitov and A. A. Kolokolov, Stationary solutions of the wave equation in a medium with nonlinearity saturation, *Izv. Vuz. Radiofiz.* **16** (1973) 1020.

28. N. G. Vakhitov and A. A. Kolokolov, *Radiophys. and Quant. Electron.* **16** (1975) 783.
29. L. Bergé, Wave collapse in physics: Principles and applications to light and plasma waves, *Phys. Rep.* **303** (1998) 259–370.
30. M. I. Molina, Nonlinear surface impurity in a semi-infinite lattice, *Phys. Rev. B* **71** (2005) 035404.
31. S. Suntsov, Discrete Surface Solitons, PhD Thesis, University of Central Florida (2007).
32. J. U. Kang, A. Villeneuve, M. Sheik-Bahae, G. I. Stegeman, K. Al-hemyari, J. S. Aitchison and C. N. Ironside, Limitation due to three photon absorption on the useful spectral range for nonlinear optics in AlGaAs below half bandgap, *Appl. Phys. Lett.* **65** (1994) 147–149.
33. A. Villeneuve, C. C. Yang, G. I. Stegeman, C.-H. Lin and H.-H. Lin, Nonlinear refractive-index near half the band gap in AlGaAs, *Appl. Phys. Lett.* **62** (1993) 2465–2467.
34. Ya. V. Kartashov, V. V. Vysloukh and L. Torner, Surface gap solitons, *Phys. Rev. Lett.* **96** (2006) 073901.
35. S. M. Jensen, The nonlinear coherent coupler, *IEEE J. Quantum Electron.* **QE-18** (1982) 1580–1583.
36. S. Nolte, M. Will, J. Burghoff and A. Tuennermann, Femtosecond waveguide writing: A new avenue to three-dimensional integrated optics, *Appl. Phys. A: Materials Science* **77** (2003) 109–111.
37. A. Bloemer, A. Szameit, F. Dreisow, T. Schreiber, S. Nolte and A. Tuennermann, Measurement of the nonlinear refractive index of fs-laser-written waveguides in fused silica, *Opt. Expr.* **15** (2006) 2151.
38. T. Pertsch, U. Peschel, F. Lederer, J. Burghoff, M. Will, S. Nolte and A. Tuennermann, Discrete diffraction in two-dimensional arrays of coupled waveguides in silica, *Opt. Lett.* **29** (2004) 468.
39. P. Yeh, *Introduction to Photorefractive Nonlinear Optics* (Wiley, New York, 1993).
40. N. K. Efremidis, S. Sears, D. N. Christodoulides, J. W. Fleischer and M. Segev, Discrete solitons in photorefractive optically induced photonic lattices, *Phys. Rev. E* **66** (2002) 046602.
41. G. Bartal, O. Cohen, H. Buljan, J. W. Fleischer, O. Manela and M. Segev, Brillouin zone spectroscopy of nonlinear photonic lattices, *Phys. Rev. Lett.* **94** (2005) 163902.
42. R. Iwanow, R. Schiek, G. Stegeman, T. Pertsch, F. Lederer, Y. Min and W. Sohler, Arrays of weakly coupled, periodically poled lithium niobate waveguide arrays: Beam propagation and discrete spatial quadratic solitons, *J. Opt. Rev.* **13** (2005) 113–121.
43. R. Iwanow, Discrete Wave Propagation in Quadratically Nonlinear Media, PhD Thesis, University of Central Florida (2005).
44. G. I. Stegeman, D. J. Hagan and L. Torner, $\chi^{(2)}$ cascading phenomena and their applications to all-optical signal processing, mode-locking, pulse compression and solitons, *J. Optical and Quant. Electron.* **28** (1996) 1691–1740.
45. C. R. Rosberg, D. N. Neshev, Y. V. Kartashov, R. A. Vicencio, W. Krolikowski, M. I. Molina, A. Mitchell, V. A. Vysloukh, L. Torner and Y. S. Kivshar, Nonlinear tamm states in periodic photonic structures, *Opt. and Phot. News* **17** (2006) 29.